Sparse Arrays and Sampling for Interference Mitigation and DOA Estimation in GNSS

Moeness G. Amin*, Xiangrong Wang*†,Yimin D. Zhang‡, Fauzia Ahmad*, and Elias Aboutanios†

***Abstract*—This paper establishes the role of sparse arrays and sparse sampling in anti-jam Global Navigation Satellite Systems (GNSS). We show that both jammer direction of arrival estimation methods and mitigation techniques benefit from the design flexibility of sparse arrays and their extended virtual apertures or coarrays. Taking advantage of information redundancy, significant reduction in hardware and computational cost materializes when selecting a subset of array antennas without sacrificing jammer nulling or localization capabilities. In addition to the spatial array sparsity, anti-jam can utilize sparsity of jammers in the spatio-temporal frequency domains. By virtue of their finite number, jammers in the field of view are sparse in the azimuth and elevation directions. For the class of frequency modulated jammers, sparsity is also exhibited in the joint time-frequency signal representation. These spatial and signal characteristics have called for the development of sparsity-aware anti-jam techniques for the accurate estimation of jammer space-time-frequency signature, enabling its effective sensing and excision. Both theory and simulation examples demonstrate the utility of coarrays, sparse reconstructions, and antenna selection techniques for anti-jam GNSS.**

***Index Terms*—GNSS, Anti-jam, sparse arrays, DOA estimation, interference mitigation.**

I. Introduction

Array processing has added significant anti-jam capabilities to Global Navigation Satellite System (GNSS) receivers. The spatial degrees of freedom (DOFs) have enabled both jammer position estimation and effective mitigation [1]–[6]. The former builds on receiving replicas of the jammer at the receiver antennas with phase difference that is a function of the jammer angle of arrival. The latter predicates on the application of spatial filtering to place nulls along the jammer directions. Combining spatial and temporal information, space-time adaptive processing (STAP) provides joint spatio-temporal processing to suppress multipath as well as narrowband and wideband interferers [7]–[10]. Polarimetric arrays utilize spatial and polarization diversities for effective suppression of jammers assuming different polarizations and angular directions [11]. Antenna arrays have also been used to improve nonstationary jammer waveform estimation and synthesis through spatial averaging and by adopting the spatial time-frequency distribution (TFD) framework [12], [13].

*Center for Advanced Communications, College of Engineering, Villanova University, Villanova, PA 19085, USA (email: {moeness.amin, fauzia.ahmad}@villanova.edu).

†School of Electrical Engineering and Telecommunications, University of New South Wales, Sydney, Australia 2052 (email:{x.r.wang, elias}@unsw.edu.au).

‡Department of Electrical and Computer Engineering, College of Engineering, Temple University, Philadelphia, PA 19122, USA (email: ydzhang@temple.edu).

The de-facto array configuration in numerous applications of array processing is the uniform linear array (ULA). In addition to ULAs, many GNSS receivers implement Controlled Radiation Pattern Antenna (CRPA) arrays [14]. ULA and CRPA arrays have, respectively, uniform distance and uniform angular spacing between neighboring antennas. Breaking these patterns by placing antennas deterministically or randomly along a continuous spatial variable or on possible grid positions establishes sparse arrays. These arrays have many advantages, including reduced redundancy, larger physical and virtual apertures, and avoidance of grating lobes [15]–[17].

Direction of arrival (DOA) estimation of jammer sources as well as GNSS satellites depends on the second-order statistics, namely, the spatial correlation matrix. The received signal correlation can be computed at all lags comprising the difference coarray, which is the set of pairwise differences of the array element positions. Accordingly, sparse arrays can be designed such that these differences span a larger set of autocorrelation lags than those of respective uniform arrays with the same number of antennas [16], [18]. This property equips GNSS receivers with the ability to estimate DOAs of many jammers in excess of the number of receiver antennas.

Jammer signals may have sparse representation in a certain single-variable or joint-variable domain. For instance, sinusoidal jammers are sparse in the frequency domain, whereas chirp jammers are sparse in the joint time-frequency (TF) domain. Exploiting signal sparsity through nonlinear reconstruction techniques improves jammer waveform estimation, leading to proper jammer excision [19], [20].

In this paper, we discuss the applications of sparse array design and sparse signal processing for jammer signal suppression and DOA estimation. We review recent results aimed at improving the performance of linear and planar arrays. It is important to note, however, that these results are easily extendable to other array structures and configurations. Although the concepts discussed here have been developed in the GNSS context, they are more widely applicable in other areas of array signal processing. We begin by reviewing, in Section II, recent developments in antenna selection techniques that maximize the beamforming signal-to-interference-plus-noise (SINR) ratio. In Section III, we address the same problem but from the DOA estimation perspective and using the Cramér-Rao bound (CRB) as a minimization criterion. In both Sections II and III, we include analysis developed in references [21]–[24] and also show two examples involving linear and planer sub-arrays. Section IV presents the coarray concept using both single and multiple CRPA receivers. It delineates the corresponding virtual aperture associated with

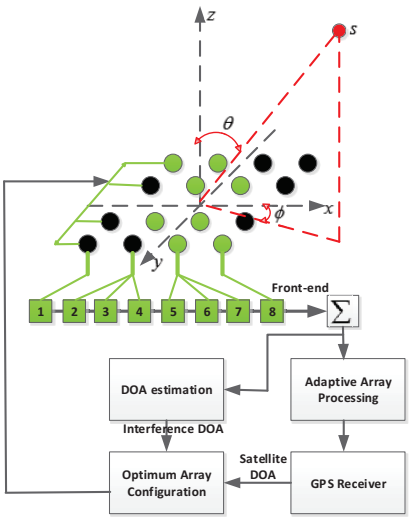

Fig. 1. Antenna array based GNSS receiver using an antenna selection strategy. The selected antennas are shown in green.

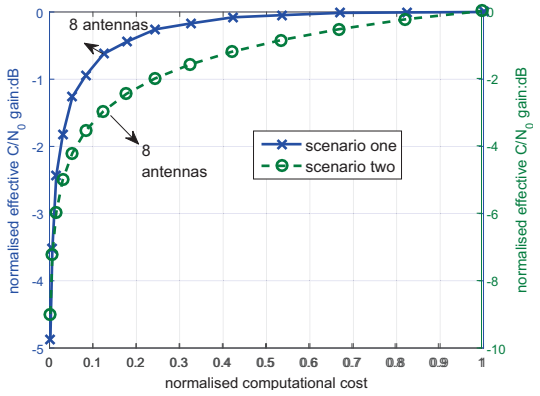

Fig. 2. Trade-off curve between the performance and the cost. The markers show the array sizes, starting with the full 16 antenna array to the right and decreasing by one at each successive point.

an already designed fixed array, where antenna selection strategies may be of limited use. We show enhanced jammer sensing using the additional DOFs and jammer spatial sparsity in the field of view. Following sensing, Section V focuses on the application of the coarray framework to jammer mitigation. Considering the fact that a large class of jammer waveforms are characterized by their instantaneous frequencies and thus exhibit sparsity in the TF domain, Section VI demonstrates effective jammer signal reconstruction and suppression under compressed observations stemming from random or missing sampling. The methods we describe in the paper have been extended to spatio-temporal processing. For example, in [25], an antenna selection approach is developed for space-time adaptive processing (STAP) in radar for clutter suppression. Similarly, in [26] and more recently [27] the time-frequency techniques have been extended to spatio-temporal processing for anti-jammer receivers. Finally, conclusions are drawn in Section VII.

II. Reconfigurable Sparse Arrays Through Antenna Selection

The array aperture size plays a fundamental role in array-based GNSS receiver performance. An increase in the aperture of a uniformly spaced array usually requires an increase in the number of antenna elements, resulting in higher hardware cost and computational complexity. Although antenna elements are becoming smaller and cheaper, the high cost of the front-end can make larger arrays very expensive [28].

Uniformly spaced arrays can exhibit significant redundancy. A non-uniform array with fewer elements can, at a fraction of the cost and complexity, provide nearly the same performance as a uniform array with the same aperture [15]. For illustration, we consider a GNSS receiver with a 4×4 planar array as shown in Fig. 1. Fig. 2 shows the effective carrier-to-noise ratio versus the computational cost for subarray sizes ranging from two antennas to the full array. The blue curve represents a scenario where the interference is close to the signal of interest and the green curve corresponds to the case where they are well separated. It is clear that an appropriately chosen subarray of 12 out of the 16 antennas can give almost the same performance as the full array for only 43% of the computation and 75% of the hardware costs. A subarray of eight antennas results in savings of 87.5% in computation and 50% in hardware for a moderate loss in performance. Therefore, optimal array thinning strategies can be useful for reducing the system cost and complexity while preserving performance.

The array configuration has usually been assumed to be fixed *a priori* and used for adaptive beamforming and filtering techniques [2]–[4]. Recent work, however, proposed a receiver architecture, shown in Fig. 1, that casts the array structure as an additional DOF in system design [29]. Antenna selection strategies, where a K-antenna subarray is chosen from the N-antenna full array, were developed to obtain the optimum subarray for any scenario [30]. Experimental results using a circular array GNSS receiver were presented in [15] to verify the effectiveness of the reconfigurable array architecture in GNSS receivers.

A. The Spatial Correlation Coefficient

The Spectral Separation Coefficient (SSC), originally proposed in [31], was extended in [21], [22] to array receivers by combining it with the Spatial Correlation Coefficient (SCC). The SCC expresses the effect of the array configuration on the receiver performance. This effect was examined in [23] for a single interference and extended in [24] to multiple interference sources. The SCC was then employed in the design of optimal arrays that maximize the separation between the signal and interference [15], [24].

Consider an N-antenna array and let $\mathbf{p}_x = [x_1, \cdots, x_N]^T$ and $\mathbf{p}_y = [y_1, \cdots, y_N]^T$ be the x and y coordinate vectors of the array elements, respectively, where $(\cdot)^T$ denotes matrix transpose. Assume L interference sources that are uncorrelated with each other and with the white noise. The spatial steering vectors of the satellite, $\mathbf{s}$, and interferences, $\mathbf{v}_j,\ j = 1, \cdots, L$, are given by

$$\mathbf{s} = e^{jk_0\mathbf{P}\mathbf{u}_s}, \quad \mathbf{v}_j = e^{jk_0\mathbf{P}\mathbf{u}_j}, \tag{1}$$

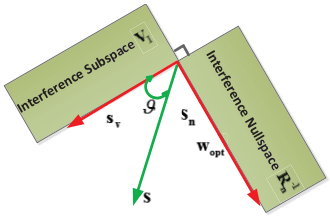

Fig. 3. The relationship between the optimum beamforming filter $\mathbf{w}_{\text{opt}}$, the interference subspace $\mathbf{V}_I$ and the nullspace $\mathbf{R}_n^{-1}$.

where $k_0 = 2\pi/\lambda$, $\mathbf{P} = [\mathbf{p}_x\ \mathbf{p}_y]$, and the DOAs are given by the $\mathbf{u}$-space parameter $\mathbf{u} = [\cos\theta\cos\phi\ \ \cos\theta\sin\phi]^T$, with ϕ being the azimuth angle and θ the elevation angle. The interference-plus-noise covariance matrix becomes

$$\mathbf{R}_n = \sigma^2\mathbf{I} + \mathbf{V}_I\mathbf{\Sigma}\mathbf{V}_I^H, \tag{2}$$

where the steering matrix $\mathbf{V}_I = [\mathbf{v}_1, \cdots, \mathbf{v}_L]$ has the interference steering vectors as its columns, $\mathbf{I}$ denotes the identity matrix, σ^2 is the noise power, and $(\cdot)^H$ denotes conjugate transpose. The diagonal matrix $\mathbf{\Sigma}$ has the interferer powers σ_j^2 arranged along its diagonal. When $\sigma_j^2 \gg \sigma^2, \forall j$, it was shown in [24] that

$$\mathbf{R}_n^{-1} \approx \frac{1}{\sigma^2}\left(\mathbf{I} - \mathbf{V}_I\left(\mathbf{V}_I^H\mathbf{V}_I\right)^{-1}\mathbf{V}_I^H\right), \tag{3}$$

approximates the interference nullspace. The optimum adaptive beamforming filter $\mathbf{w}_{\text{opt}} = \gamma\mathbf{R}_n^{-1}\mathbf{s}$, where γ is a constant, is then approximately equal to the projection of the satellite steering vector $\mathbf{s}$ onto the interference nullspace. The SCC, α, is then defined as the cosine of the angle ϑ between the signal and the interference subspace, as shown in Fig. 3. Assuming without loss of generality $\|\mathbf{s}\|_2 = \sqrt{N}$, the squared SCC is expressed in terms of the determinants of two matrices,

$$|\alpha|^2 = 1 - \frac{|\mathbf{D}_s|}{\|\mathbf{s}\|_2^2|\mathbf{D}_I|} = 1 - \frac{|\mathbf{D}_s|}{N|\mathbf{D}_I|}, \tag{4}$$

where

$$\mathbf{D}_I = \mathbf{V}_I^H\mathbf{V}_I, \text{ and } \mathbf{D}_s = \mathbf{V}_s^H\mathbf{V}_s. \tag{5}$$

with $\mathbf{V}_s = [\mathbf{s}, \mathbf{V}_I]$. The signal-to-noise ratio (SNR) at the output of the adaptive filter is given in terms of the SCC as [24],

$$\rho_{\text{out}} = \sigma_s^2\mathbf{s}^H\mathbf{R}_n^{-1}\mathbf{s} = \rho_{in}\cdot N(1-|\alpha|^2), \tag{6}$$

where σ_s^2 is the signal power and ρ_{in} is the input SNR. We see that ρ_{out} depends on both the number of available antennas N and the squared SCC. Thus, for fixed N, the performance can be improved by changing the array configuration to reduce the SCC value. Alternatively, a reduction in the number of antennas can be compensated by a suitable design of the antenna configuration to reduce the SCC. Observe that if the DOAs of the interference sources are mutually orthogonal, i.e., $\mathbf{v}_i^H\mathbf{v}_j = 0, \forall i \neq j$, then

$$|\alpha|^2 = \sum_{j=1}^{L}\frac{|\mathbf{s}^H\mathbf{v}_i|^2}{(\mathbf{s}^H\mathbf{s})(\mathbf{v}_j^H\mathbf{v}_j)} = \sum_{j=1}^{L}|\alpha_j|^2. \tag{7}$$

Here, α_j is the SCC value of the desired signal and the jth interference. The squared SCC value becomes the sum of the squared SCCs of the individual interference sources. In the case of single interference as in [15], the squared SCC in Eq. (4) reduces to

$$|\alpha|^2 = \frac{|\mathbf{s}^H\mathbf{v}|^2}{\|\mathbf{s}\|_2^2\|\mathbf{v}\|_2^2} = \frac{|\mathbf{s}^H\mathbf{v}|^2}{N^2}, \tag{8}$$

where $\mathbf{v}$ denotes the steering vector of the single interference.

B. The Antenna Selection Strategy

The optimum subarray selection based on the minimization of the SCC for the single interference case was provided in [15]. Let $\mathbf{x}$ be a length-N selection vector with an entry of 1 indicating that the antenna element at the corresponding position is selected, and 0 otherwise. The steering vectors with respect to the subarray are $\tilde{\mathbf{s}} = \mathbf{x}\odot\mathbf{s}$ and $\tilde{\mathbf{v}} = \mathbf{x}\odot\mathbf{v}$, where $\odot$ denotes element-wise product, and

$$|\alpha|^2 = \frac{|\tilde{\mathbf{s}}^H\tilde{\mathbf{v}}|^2}{\|\tilde{\mathbf{s}}\|_2^2\|\tilde{\mathbf{v}}\|_2^2}. \tag{9}$$

Defining the vector $\tilde{\mathbf{w}} = \mathbf{s}\odot\mathbf{v}$, the squared SCC of the selected K-antenna subarray is rewritten as,

$$|\alpha|^2 = \frac{\mathbf{x}^T(\tilde{\mathbf{w}}\tilde{\mathbf{w}}^H)\mathbf{x}}{K^2}. \tag{10}$$

The antenna selection problem is then cast as a two-way partitioning model [32] as follows:

$$\begin{aligned} \min_{\mathbf{x}}\quad & |\alpha|^2 \\ \text{s.t.}\quad & x_i(x_i-1) = 0, \quad i = 1, ..., N, \\ \text{and}\quad & \mathbf{1}^T\mathbf{x} = K, \end{aligned} \tag{11}$$

where $\mathbf{1}$ is a vector of all ones. Eq. (11) can be solved using the Correlation Measurement (CM) method [33], which applies a simple greedy search approach. Specifically, in every iteration, it removes the antenna with the largest total correlation relative to all remaining elements in order to reduce the candidate set size.

The CM method cannot control the subarray response, possibly resulting in high sidelobes and grating lobes. In contrast, the Difference of Convex Sets (DCS) method, which replaces the binary constraint by an equivalent difference of two convex sets, allows a beampattern to be specified as SCC values on a DOA sampling grid. This is then solved using an iterative algorithm that terminates when the difference between two successive solutions becomes sufficiently small.

The optimization problem for optimum subarray selection in the presence of multiple interferers is cast as the minimization

$$\begin{aligned} \min_{\mathbf{x}}\quad & 1 - \frac{|\tilde{\mathbf{D}}_s|}{K|\tilde{\mathbf{D}}_I|} \\ \text{s.t.}\quad & x_i(x_i-1) = 0, \quad i = 1, ..., N, \\ & \mathbf{1}^T\mathbf{x} = K, \end{aligned} \tag{12}$$

where $\tilde{\mathbf{D}}_I = \mathbf{V}_I\text{diag}(\mathbf{x})\mathbf{V}_I$ and $\tilde{\mathbf{D}}_s = \mathbf{V}_s\text{diag}(\mathbf{x})\mathbf{V}_s$ are positive definite, and $\text{diag}(\mathbf{x})$ is a diagonal matrix with the vector $\mathbf{x}$

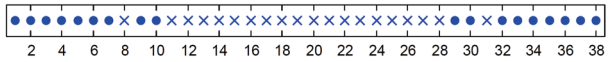

(a) 18-antenna optimum subarray 1 selected by subspace based SCC ('sub$_1$')

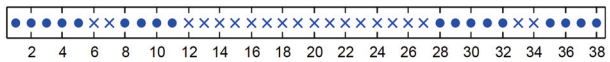

(b) 18-antenna optimum subarray 2 selected by sum of SCC ('sub$_2$')

Fig. 4. The selected subarrays, with the chosen antennas shown as points.

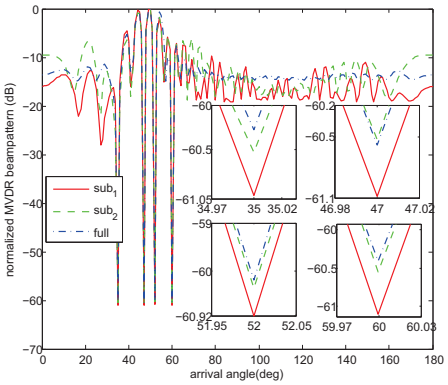

Fig. 5. Minimum variance distortionless response beampatterns of the full array and two optimum subarrays. The number of time snapshots is 100.

populating its diagonal. This is equivalent to,

$$\begin{aligned} \min_{\mathbf{x}} \quad & \log(|\tilde{\mathbf{D}}_I|) - \log(|\tilde{\mathbf{D}}_s|), \\ \text{s.t.} \quad & x_i(x_i - 1) = 0, \quad i = 1, ..., N, \\ & \mathbf{1}^T\mathbf{x} = K, \end{aligned} \tag{13}$$

which is a Difference of Convex (D.C.) Programming problem [34] and is solved in [30] using a convex-concave procedure.

To show the performance of the antenna selection strategy, we consider four interferers, all having interference-to-noise ratio (INR) of 30 dB and arriving from azimuth angles $52°, 47°, 60°$, and $35°$. We select 18 antennas from a 38-antenna ULA. Fig. 4 shows the performance of two subarrays: "sub$_1$" is obtained from (13), whereas "sub$_2$" is derived from (7) which assumes the sources to be mutually orthogonal. The associated beampatterns of the two subarrays are depicted in Fig. 5. Note that "sub$_1$" exhibits the same mainlobe width and peak sidelobe level (SLL) as the full array but deeper nulls. On the other hand, "sub$_2$" shows poorer performance due to the orthogonality assumption being invalid. The increased null depths produced by "sub$_1$" are due to the fact that the interferences and satellite signal of interest are "more orthogonal" with respect to the selected subarray.

The applicability of the above method to anti-jam GPS receivers requires either multiplexing among different subarrays, each is optimum for one satellite, or solving the optimization problems (9) and (10) involving the SCC of all satellites in the field of view.

III. Enhanced DOA Estimation with Adaptively Thinned Arrays

Beside interference mitigation, antenna selection strategies were developed in [35] for DOA estimation with arbitrarily shaped arrays using the CRB criterion. This essentially

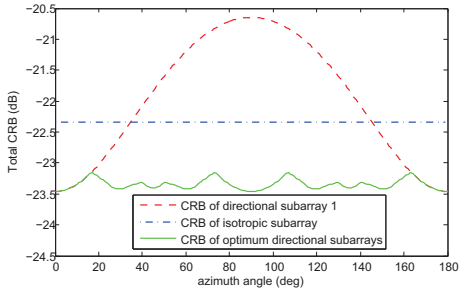

Fig. 6. Total CRB versus azimuth angle. The SNR is 10 dB.

involves the minimization of the trace of $\mathbf{C}_F$, denoted as $\text{tr}(\mathbf{C}_F)$, with $\mathbf{C}_F$ being the inverse of the Fisher information matrix (FIM). Both isotropic and directional subarrays were considered. In the absence of *a priori* knowledge of the DOAs, an isotropic subarray, that is, a subarray with the same CRB for all DOAs, should be used. If a particular direction is of interest, we seek a directional array that minimizes the CRB at that DOA. As there is inherently a trade-off between the minimization of the CRB and SLL control for non-uniform subarrays, the SCC is incorporated into the optimization procedure to enable control of the SLL. This is again done by specifying SCC values on a DOA sampling grid.

In order to formulate the antenna selection problem, the FIM is expressed in terms of the selected antenna position vectors, $\tilde{\mathbf{p}}_x = \mathbf{x} \odot \mathbf{p}_x$ and $\tilde{\mathbf{p}}_y = \mathbf{x} \odot \mathbf{p}_y$, where $\mathbf{p}_x$ and $\mathbf{p}_y$ are defined in the previous section and $\mathbf{x}$ is the binary selection vector. The goal in the isotropic array case is to minimize $\text{tr}(\mathbf{C}_F)$ while constraining the off-diagonal entries of the FIM to 0. Relaxing the binary constraint using the DCS method allows the problem to be solved in polynomial time [35].

For directional subarrays, the constraint on the off-diagonal elements of the FIM is removed and $\text{tr}(\mathbf{C}_F)$ is minimized. This was recast as the minimization of the ratio of the traces of two matrices. A Dinklebach-type algorithm [36] was proposed in [35] for adaptive directional subarray selection.

The performance of the two methods is shown in Fig. 6. A 10-antenna subarray is chosen from a planar 5×5 array. For the simulation, the elevation is set to $10°$ and the azimuth is swept from $0°$ to $180°$. A directional subarray focused at $0°$ azimuth, depicted by the red curve, exhibits degraded performance at other angles. In contrast, it is clear from the green curve that optimal directional subarrays, where the optimal subarray is chosen for each azimuth, provide the best performance across the entire DOA range. The isotropic array, shown by the blue curve, compromises the CRB in order to attain identical performance across all azimuth angles.

IV. Coarray Based Sparse Geometries for DOA Estimation with Multiple CRPA Arrays

In this section, we consider multiple CRPA GNSS arrays that have a circular aperture with one element at the center and three to seven on the circumference. Guided by the coarray formalism, we design sparse placements of multiple CRPA arrays on a regular Cartesian grid to permit DOA estimation

of a number of interferers much higher than the number of physical antennas.

A. Difference Coarray

The difference coarray is defined as the set of pairwise differences of the physical array element positions [16]. This difference set occurs naturally in the computation of the second-order statistics, such as the spatial covariance matrix of a signal received by an N-element array. Thus, applications relying on second-order statistics, such as DOA estimation, can exploit all the DOFs offered by the difference coarray. Assume that the positions of the array elements form the set

$$\mathbb{P} = \{\mathbf{p}_i = (m_i, n_i)d_0 : i = 1, \cdots, N\}, \tag{14}$$

for non-negative integers m_i and n_i, and d_0 is the fundamental unit inter-element spacing (usually one-half wavelength). The corresponding difference coarray has positions,

$$\mathbb{P}_d = \{\mathbf{p}_i - \mathbf{p}_j : i, j = 1, \cdots, N\}. \tag{15}$$

The received signal correlation can be calculated at all "lags" comprising the difference coarray. Hence, by suitable construction of the original set $\mathbb{P}$, the number of spatial lags can be substantially increased for a given number N of physical antennas. An example of such an array structure is minimum redundancy linear array (MRLA) [37]. Given N physical antennas, an MRLA aims at minimizing the number of redundant lags without introducing any missing lags or "holes" in the difference coarray. For illustration, a 4-element MRLA with element positions $\mathbb{P} = \{0, 1, 4, 6\}d_0$ generates a uniformly spaced difference coarray with element positions $\mathbb{P}_d = \{-6, -5, \cdots, 5, 6\}d_0$.

B. Sparse Geometries of Multiple CRPA GNSS Arrays

We first consider a single CRPA array consisting of eight antennas, with one antenna in the center and the remaining seven uniformly distributed along the circumference of a circle with radius one wavelength, as indicated by the magenta filled circles in Fig. 7. Its difference coarray, represented by the green circules in Fig. 7, comprises four concentric circular arrays, each having 14 uniformly distributed virtual elements, plus one virtual antenna in the center. The resulting total number of distinct spatial lags is $N(N-1)+1 = 57$, including both positive and corresponding negative lags. In case of multiple CRPA arrays, the corresponding difference coarray consists of not only the self-differences between the elements of the same CRPA array, but also the cross-differences between the elements of different CRPA arrays. Unlike conventional two-dimensional (2-D) non-uniform array design, the sparse configuration design using multiple CRPA arrays imposes additional constraints due to the circular nature of each CPRA array. With this restriction, we consider each CRPA array as a unit element and design sparse placements of multiple CPRA arrays on a regular Cartesian grid such that the cross-differences have minimum or reduced redundancy and are distinct from the self-differences.

More specifically, consider the placement problem of four 8-element CRPA arrays. The "linear" configuration that provides minimally redundant cross-differences and no overlap with the self-differences is based on a 4-antenna MRLA structure. This configuration and its corresponding coarray are shown in Fig. 8 by the magenta and green circles, respectively. The center-to-center distance between the various CRPA arrays in the designed configuration equals four wavelengths, which is approximately the diameter of the difference coarray corresponding to a single CRPA array. We observe that, in addition to the four concentric virtual arrays generated by the self-differences of each CPRA array, there are nine additional concentric arrays corresponding to the cross-differences. In total, 741 distinct spatial lags (positive and negative) are generated in the coarray.

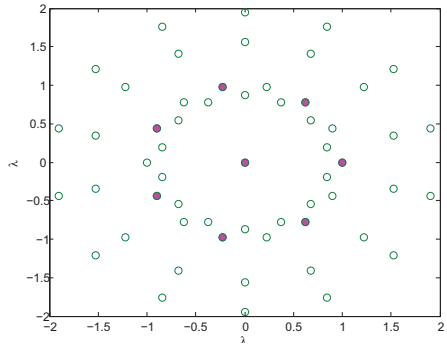

Fig. 7. A single CRPA array with center element (magenta filled circles) and its corresponding difference coarray (green circles).

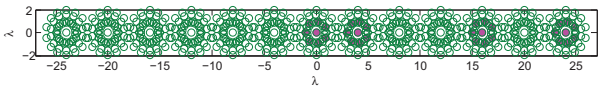

Fig. 8. MRLA configuration of four CRPAs and the corresponding coarray.

Next, we arrange the four CRPA arrays into a 2-by-2 boundary configuration with a center-to-center spacing of 4 wavelengths, as shown in Fig. 9. The corresponding coarray consists of nine concentric virtual arrays arranged as a 3-by-3 square. There are a total of 513 distinct positive and negative spatial lags in the coarray. Clearly, both MRLA based and boundary sparse configurations of multiple CRPA arrays produce coarrays with much higher number of DOFs than the physical array. This enables accurate localization of a significantly larger number of interferers than the physical aperture permits. Note that the two sparse structures offer different resolution capabilities in azimuth and elevation.

C. DOA Estimation Using Multiple CRPA Arrays

In order to fully exploit the enhanced DOFs offered by the coarrays of the sparse configurations, DOA estimation should proceed within the coarray framework. There are two approaches that utilize coarrays for high-resolution DOA estimation, namely, covariance augmentation [17], [38] and covariance vectorization [18]. As the former requires complicated matrix completion to guarantee the positive definiteness of the augmented Toeplitz matrix [39], we focus here on the latter technique.

Let us consider L narrowband jammers and K satellite

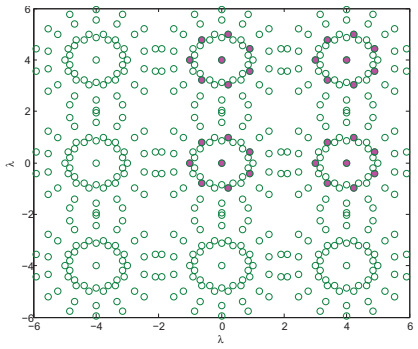

Fig. 9. Boundary configuration of four CRPAs and the corresponding coarray.

signals impinging on an N-antenna array ($L > N$). All L jammers and K satellite signals are assumed to be uncorrelated with each other. Let the steering vector of the lth jammer be denoted by $\mathbf{v}_l$ and that of the kth satellite be $\mathbf{s}_k$. These are defined according to (1). In what follows, we use the subscripts j and s to specify the parameters of a jammer and satellite respectively. Then, the correlation matrix $\mathbf{R}_x$ of the signal plus noise is given by

$$\mathbf{R}_x = \mathbf{V}\mathbf{R}_s\mathbf{V}^H + \sigma^2\mathbf{I}, \tag{16}$$

where the array manifold matrix $\mathbf{V} = [\mathbf{v}_1, \cdots, \mathbf{v}_L, \mathbf{s}_1, \cdots, \mathbf{s}_K]$, and $\mathbf{R}_s$ represents the source correlation matrix, which is a diagonal matrix with the source powers $\sigma^2_{j1}, \cdots, \sigma^2_{jL}, \sigma^2_{s1}, \cdots, \sigma^2_{sK}$ along its diagonal. The (i,j)th element of $\mathbf{R}_x$ is,

$$\begin{aligned}[\mathbf{R}_x]_{ij} &= \sum_{k=1}^{K} \sigma^2_{jk} e^{jk_0 d_0((m_i-m_j)\mu_k + (n_i-n_j)\nu_k)} + \sigma^2\delta(i-j) \\ &+ \sum_{l=1}^{L} \sigma^2_{sl} e^{jk_0 d_0((m_i-m_j)\mu_{sl} + (n_i-n_j)\nu_{sl})},\end{aligned} \tag{17}$$

where $\delta(i-j)$ is the Kronecker Delta function, and $\mathbf{u} = [\mu, \nu]^T$ is the $\mathbf{u}$-space parameter. It is clear that $[\mathbf{R}_x]_{ij}$ can be treated as the data received by the coarray element position $(m_i - m_j, n_i - n_j)d_0$.

Vectorizing $\mathbf{R}_x$, we obtain

$$\tilde{\mathbf{y}} = \text{vec}(\mathbf{R}_x) = \tilde{\mathbf{V}}\mathbf{b} + \sigma^2\tilde{\mathbf{i}}, \tag{18}$$

where $\tilde{\mathbf{V}} = \mathbf{V}^* \otimes \mathbf{V}$ with $\otimes$ denoting Khatri-Rao product, $\mathbf{b} = [\sigma^2_{j1}, \cdots, \sigma^2_{jL}, \sigma^2_{s1}, \cdots, \sigma^2_{sK}]^T$ and $\tilde{\mathbf{i}} = \text{vec}(\mathbf{I})$. The vector $\tilde{\mathbf{y}}$ can be viewed as a single snapshot received by the difference coarray. Utilizing the coarray measurement vector $\tilde{\mathbf{y}}$ for DOA estimation permits exploitation of the enhanced DOFs offered by the coarray. The equivalent source signal $\mathbf{b}$ consists of the source powers and the noise becomes a deterministic vector. Therefore, the rank of the covariance matrix of $\tilde{\mathbf{y}}$ is one and subspace-based DOA estimation techniques, such as MUSIC, would fail. In this case, sparse reconstruction based direction finding can be employed. It should be noted that if the coarray has no holes and its elements lie on a uniform grid, spatial smoothing can be utilized to restore the rank of the covariance matrix [40]. Subsequently, either interference spectrum based DOA estimation approaches or polynomial rooting methods, both employing the smoothed coarray covariance matrix, can be used instead of sparse reconstruction approach. The search-free polynomial rooting method exhibits two main advantages, namely, reduced computational complexity and off-grid DOA estimation, over the interference spectrum and sparse reconstruction methods.

For the sparse reconstruction based DOA estimation [41], the estimates of $\mathbf{b}$ and σ^2 are obtained as the solution to an l_1-norm regularization problem. For notational compactness, we define $\bar{\mathbf{V}} = [\tilde{\mathbf{V}}, \tilde{\mathbf{i}}]$ and $\bar{\mathbf{b}} = [\mathbf{b}, \sigma^2]$. Then, (18) can be rewritten as,

$$\tilde{\mathbf{y}} = \bar{\mathbf{V}}\bar{\mathbf{b}}. \tag{19}$$

By defining a dictionary matrix $\bar{\mathbf{V}}^d$ as the collection of coarray steering vectors over a searching grid with $Q > L$ points, the l_1-norm regularization problem can be formulated as,

$$\bar{\mathbf{b}}^d = \text{argmin}_{\mathbf{z}} \left\{ \|\tilde{\mathbf{y}} - \bar{\mathbf{V}}^d\mathbf{z}\|_2 + \rho\|\mathbf{z}\|_1 \right\}. \tag{20}$$

Here, the solution vector $\bar{\mathbf{b}}^d$ is sparse with L obviously larger entries than the remaining ones, as jammers are much stronger than both satellite signals and noise. The l_2-norm in the objective function denotes the least square cost function ensuring data fidelity, and the l_1-norm promotes the sparsity of the solution. In addition, ρ is the trade-off parameter between the least square error and the solution sparsity. The above optimization problem is convex and can be effectively solved by a variety of methods, such as convex programming [32] for problems of moderate size and complex variants of LASSO [42] for large scaled problems. It is noted that the sparse reconstruction methods are sensitive to coherency of the dictionary matrix $\bar{\mathbf{V}}^d$ and the determination of the trade-off parameter ρ is still an open problem [43], [44]. Alternatively, Bayesian compressive sensing, which is more robust to dictionary coherence, can be utilized for DOA estimation using the difference coarray. Interested readers are referred to [30] for detailed formulation of the Bayesian approach.

As an illustrative example of the coarray based DOA estimation using multiple CRPA arrays, we first consider the "linear" structure of Fig. 8. We assume 70 jammers uniformly distributed within the $[10^\circ, 355^\circ]$ azimuth sector with 5° increment at 0° elevation, all having an INR of 20 dB. The sensing spectrum of the coarray based sparse reconstruction approach is depicted in Fig. 10. We can see that all 70 sources have been successfully identified. However, some spurious peaks are also observed and large bias appears in the vicinity of the endfire directions of $0^\circ, 180^\circ$ and 360°. The latter issue is inherited from "linear" arrays.

On the other hand, the boundary configuration depicted in Fig. 9, fails to estimate all 70 jammers correctly due to its decreased number of spatial lags, as seen in Fig. 11 (top plot). Next, we consider 40 jammers uniformly distributed within the azimuth sector of $[20^\circ, 332^\circ]$ with 8° increment at 0° elevation, all having an INR of 20 dB. The sensing spectrum obtained with the boundary array is shown in the bottom plot of Fig. 11, where the jammer DOAs have been correctly estimated.

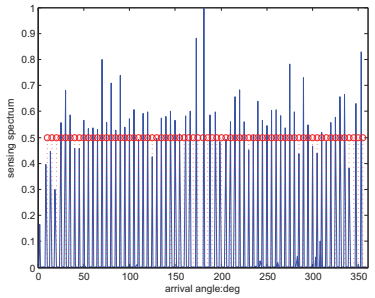

Fig. 10. Sensing spectrum of the coarray depicted in Fig. 8.

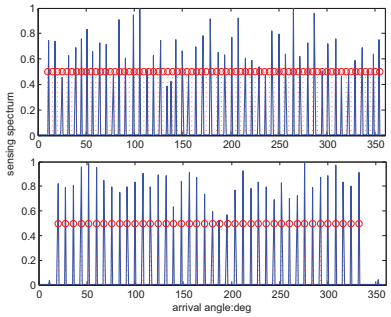

Fig. 11. Sensing spectrum of the coarray depicted in Fig. 9.

V. Interference Suppression Within the Coarray Framework

GNSS receivers are vulnerable to the presence of jammers and interferences. In order to counter this problem, a number of anti-jam techniques have been developed based on the spatial and temporal DOFs [4], [26], [45], [46]. Multiple antenna receivers allow the implementation of spatial nulling and beamsteering based on adaptive beamforming and high-resolution DOA estimation methods. Adaptive interference nulling algorithms based on antenna arrays can be broadly classified into two types, namely, open-loop and closed-loop techniques. The open-loop null-steering algorithms involve a two-step procedure [47]. First, the DOAs of all signals impinging on the array are estimated. Second, a set of complex weights is computed which places proper nulls in the estimated interference directions. In this regards, accurate interference DOA estimates would imply better jammer suppression.

Typical high-resolution DOA estimation techniques are those evolving around Capon's method and MUSIC algorithm. However, the number of estimated signals cannot exceed the number of physical antennas. This may present a challenge for GNSS receivers, stemming from their limited number of antennas. As such, coarray-based DOA estimation can be utilized for detecting a high number of jammers that may exceed the number of physical antennas. One such approach, namely the coarray-based sparse reconstruction, was discussed in Section IV-C and can be utilized to sense the interference environment in the GNSS receivers field of view. However, the coarray based processing does not directly lend itself to interference nulling as in the case of physical arrays. Therefore, all potential jammers should be subsequently identified and their strengths should be determined. Stronger and more deleterious jammers can then be suppressed using methods such as subspace projection [48].

For illustration, consider the 8-element CRPA array shown in Fig. 7. Suppose there are 10 jammers arriving from $[10^\circ, 20^\circ, 30^\circ, 10^\circ, 20^\circ, 30^\circ, 10^\circ, 20^\circ, 30^\circ, 38^\circ]$ in elevation and uniformly distributed in $[30^\circ, 300^\circ]$ azimuth sector with 30° increment. The corresponding INR values are $[10, 20, 10, 20, 20, 10, 20, 20, 30, 20]$ dB. Two satellites, SVN-5 and SVN-10, are viewed from $[30^\circ, 60^\circ]$ and $[15^\circ, 120^\circ]$ in elevation and azimuth, respectively, with equal SNR of 10 dB. The Doppler frequency and Coarse/Acquisition (C/A) code shift of SVN-8 are 1.5 kHz and 800 chips, while those of SVN-10 are 1 kHz and 600 chips. The interfering jammers are first estimated by utilizing the coarray based sparse reconstruction approach. The DOA estimates are shown in Fig. 12, where the elevation is plotted along the radius and the azimuth on the circumference. We can observe that the estimated angles coincide with the true angles, which further validates the effectiveness of the coarray based approach. Seven strong jammers are identified from the sparse reconstruction based sensing spectrum and excised from the received signal by projecting it onto jammers' orthogonal subspace. The acquisition processing is then applied to the signal after mitigation of strong jammers. The acquired Doppler frequency and C/A code phase shift of the SVN-10 and SVN-5 are clearly indicated in Fig. 13 and Fig. 14, respectively.

For comparison, a traditional direct implementation of minimum output power (MOP) based on physical array is also utilized for interference suppression [7]. More specifically, we simply constrain the weight of the first antenna, and then minimize the output power without attempting to preserve the gain in the signal direction. This method has the disadvantage of allowing for possible signal fades, but enjoys the advantage of not requiring the user to know the expected DOA of the incoming satellite signal. The optimization formulation of the MOP criterion is,

$$\min_{\mathbf{w}} \mathbf{w}^H \mathbf{R}_x \mathbf{w} \quad \text{subject to } \mathbf{w}^H \tilde{\mathbf{f}} = 1. \tag{21}$$

Here $\tilde{\mathbf{f}} = [1, 0, \cdots, 0]^T \in \mathbb{R}^N$. Implementing Lagrange Multiplier yields,

$$\mathbf{w}_{\mathrm{c}} = \mu \mathbf{R}_x^{-1} \mathbf{f}, \tag{22}$$

where μ is a constant scalar. As the number of jammers exceeds that of physical antennas, the traditional MOP anti-jam approach fails, as confirmed by the acquisition performance for SVN-10 in Fig. 15.

VI. Sparse Sampling

Commonly used jammers are frequency modulated (FM) signals which are characterizable as instantaneously narrowband. Depending on how their instantaneous frequencies (IFs) vary with time, such FM jammers range from chirp-like waveforms to higher-order polynomial phase signals. In this section, we address jammer suppression based on jammer waveform estimation and temporal domain suppression. Of particular interest is the case when a substantial portion of the

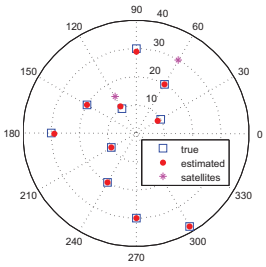

Fig. 12. 2-D DOA estimation: the square and circle indicate the true and estimated jammer directions, respectively. The two satellites are indicated by asterisks.

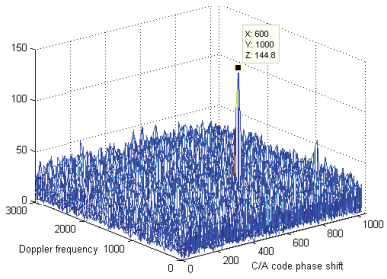

Fig. 13. Acquisition performance of the SVN-10 using coarray-based open-loop approach.

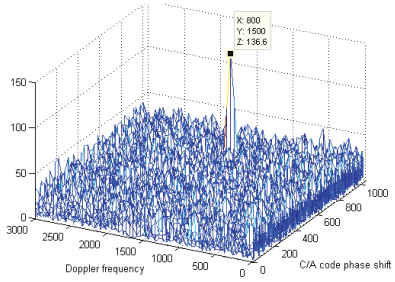

Fig. 14. Acquisition performance of the SVN-5 using coarray-based open-loop approach.

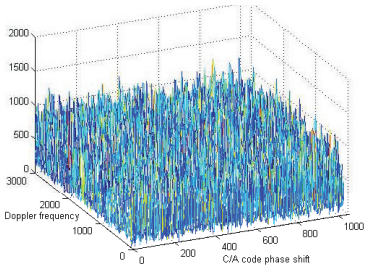

Fig. 15. Acquisition performance of the SVN-10 using MOP based on physical arrays.

data samples is missing, rendering the conventional jammer waveform estimation methods ineffective.

FM jammers cannot be simply mitigated by windowing or filtering because they usually occupy the entire GNSS signal bandwidth and span a large portion, or the entire period, of the time. An effective approach to achieve jammer waveform estimation and suppression is through accurate estimation of the jammer IFs, and joint-variable signal representations in the TF domain are often used to reveal the jammer signatures due to their power concentrations in the IF ridges [49]. In this case, jammer excision becomes a two-step process. The first step is to estimate the TF signature or the IF of the jammer, whereas the second step is to perform excision based on such estimates. Both steps can be performed as a pre-processing prior to the correlation and despreading procedures of a GNSS receiver. A number of methods have also been developed for parametric estimations and synthesis of FM jammer signals in which the jammer polynomial phase characteristics are utilized [50], [51]. For the second step, some of the temporal anti-jam techniques proceed to subtract the jammer from the received data, and it is more common to perform data projection on the null space of the jammer to avoid performance degradation with signal subtraction when the phase estimation errors are not negligible [26].

Traditional anti-jam GNSS receivers assume the received signals to be uniformly sampled at the chip rate or over-sampled above the chip rate of the spreading codes. In real-world operations, however, jammed GNSS signal samples may be randomly missing due to various reasons. Consider an impulsive noise present in the data in conjunction with an FM jammer [52]. In this case, it becomes difficult to provide an accurate jammer estimate due to the highly contaminating impulsive noise. Discarding the high amplitude data samples can remove most of the impulsive noise, rendering the data "incomplete" or randomly sampled [53]. Impulsive noise sources may, for example, include motor ignition noise, which is generated by spark plugs used in internal combustion engines, impulsive and noise-like waveforms generated by radar systems, and ultrawideband emitters. Obstructed line-of-sight may also yield random highly attenuated or missing samples.

Missing samples generate noise-like artifacts in the TF domain representations, making conventional approaches for anti-jam infeasible. Waveform recovery and/or IF estimation of FM signals from sparsely sampled observations fall under the emerging area of compressive sensing and sparse reconstruction [19], [53], [54]. Owing to their instantaneous narrowband characteristics, these signals exhibit local sparsity when viewed through a short window or when they, in general, are represented in the joint-variable TF domain. Such sparsity property invites compressive sensing and sparse reconstruction techniques to play a role in anti-jam GNSS. In [53], the effect of missing samples on bilinear TFDs is analyzed. IF estimation based on applying a signal-dependent adaptive optimal kernel (AOK) together with sparse signal reconstruction is described.

In this section, we address compressive sensing-based approach for accurate IF estimation and excision of jammers from incomplete signal observations [20]. Jammer TF signature estimation is achieved by exploiting the fact that the FM jammers are locally sparse in the TF domain due to their power localizations at and around their IFs. Reconstruction of such jammer signals from few random observations falls under the emerging area of compressive sensing [19], [53], [55]. Note that, when the observed signals do not have missing samples, the compressive sensing-based techniques still show improvement over the non-sparsity-aware techniques. Compressive sensing-based techniques are particularly attractive

when the jammers cannot be parameterized and conventional jammer waveform estimation methods become ineffective.

A. Signal Model

GNSS signals and the associated jammers adhere to the narrowband signal model. Consider a situation where K GNSS signals $s_k(t), k = 1, \cdots, K$, are contaminated by L jammer signals $v_l(t), l = 1, \cdots, L$. Then, the discrete-time received signal vector can be expressed as

$$y(t) = \sum_{k=1}^{K} h_k s_k(t) + \sum_{l=1}^{L} h_l v_l(t) + n(t) \tag{23}$$

for $0 \leq t \leq T-1$, where h_k and h_l are the respective channel coefficients for the kth GNSS signal and the lth jammer. The jammer signals $v_l(t), l = 1, \cdots, L$, are assumed to be FM with unit power. In addition, $n(t)$ is the additive white Gaussian noise $\mathcal{CN}(0, \sigma_n^2)$. Note that t is discretized with a sampling interval of Δt.

Consider sparse sampling of the observations with a random pattern. As such, the sparse observation is given as

$$x(t) = y(t) \cdot b(t), \tag{24}$$

where $b(t) \in \{0, 1\}$ is a binary mask, and the data at time t is missing when $b(t) = 0$.

B. Time-Frequency Representations

A signal can be quadratically represented as joint-variable in the TF domain, instantaneous autocorrelation function (IAF) domain, and the ambiguity function (AF) domain. The IAF of signal $x(t)$ is defined for time lag τ as

$$C(t, \tau) = x(t + \tau)x^*(t - \tau). \tag{25}$$

The Wigner-Ville distribution (WVD) is known as the simplest form of a TFD. The WVD is the Fourier transform of the IAF with respect to τ, expressed as

$$W(t, f) = \mathcal{F}_\tau[C(t, \tau)] = \sum_{\tau} C(t, \tau) e^{-j4\pi f \tau}, \tag{26}$$

where f represents the frequency. Note that 4π is used in the discrete-time Fourier transform (DFT) instead of 2π because the time-lag τ takes integer values in (25). On the other hand, the inverse DFT (IDFT) of the IAF with respect to t yields the AF, expressed as

$$A(\zeta, \tau) = \mathcal{F}_t[C(t, \tau)] = \sum_{t} C(t, \tau) e^{-j2\pi f t}, \tag{27}$$

where ζ is the frequency shift or Doppler.

It is clear that WVD maps one-dimensional (1-D) signal $x(t)$ in the time domain into 2-D signal representations in the TF domain. The fundamental TFD property of concentrating the FM jammer energy at and around its IF, while spreading the GNSS signal and noise energy over the entire TF domain, enables effective jammer and GNSS signal separations when considering the time and frequency variables jointly.

For illustration purposes, we consider two FM jammers that impinge on the receiver along with a C/A code GPS signal. The IFs of the two FM jammers are expressed as,

$$f_1(t) = 0.05 + 0.1t/T + 0.3t^2/T^2, \tag{28}$$
$$f_2(t) = 0.15 + 0.1t/T + 0.3t^2/T^2, \tag{29}$$

for $t = 1, ..., T$, where the block size of the signal is chosen to be $T = 128$, and each sample corresponds to a chip interval. The input SNR of the GPS signal is -16 dB, and the input INR is 25 dB. In Fig. 16, we show the real-part waveform and the magnitudes of the WVD, AF, and IAF of the two-component jammer. While the jammer IFs are clearly observed in the WVD, it also shows strong cross-terms between the two jammer components, as well as those between the same components due to the nonlinear IF signatures.

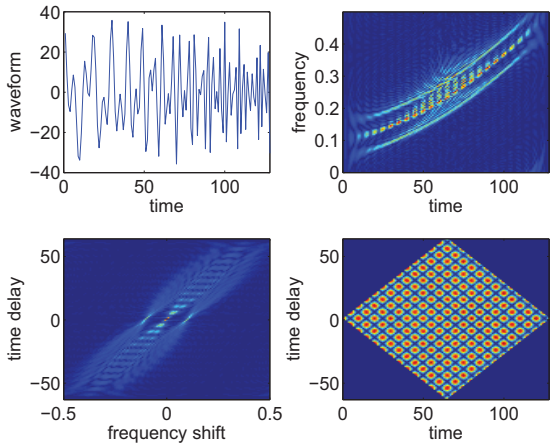

Fig. 16. Real-part waveform, WVD, AF, and IAF of a two-component jammer without missing samples.

1) Effect of Missing Samples: Missing time-domain samples generate missing entries in the IAF and, as a result, yield noise-like artifacts in the WVD as well as the AF domain. To understand such effects, we depict in Fig. 17 the same plots as in Fig. 16, but with 50% (or 64) randomly missing data samples. The missing data positions are marked with red dots in Fig. 17(a). It is clear that both WVD and AF are cluttered by the artifacts due to missing data samples.

2) Time-Frequency Kernels: WVD is often regarded as the basic or prototype quadratic TFDs, since other quadratic TFDs can be described as filtered versions of the WVD. WVD is known to provide the best TF resolution for single-component linear FM signals, but it yields high cross-terms when the frequency law is nonlinear or when a multi-component signal is considered. Various reduced interference kernels have been developed to reduce the cross-term interference [56]. As such, the properties of a TFD can be characterized by the constraints on the kernel. Different kernels have been designed and used to generate TFDs with prescribed, desirable properties. While some kernels assume fixed (signal-independent) parameters, other kernels, such as the AOK, provide signal-adaptive filtering capability [57].

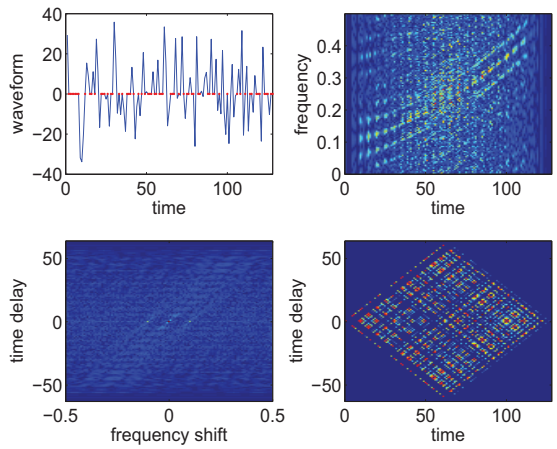

Fig. 17. Real-part waveform, WVD, AF, and IAF of the two-component jammer with 50% missing samples. The red dots in the waveform show the missing data positions.

The AOK is obtained by solving the following optimization problem for AF $A(r,\psi)$ defined in the polar coordinates [57]:

$$\begin{aligned} &\max_{\Phi} \int_0^{2\pi}\int_0^{\infty} |A(r,\psi)\Phi(r,\psi)|^2 \, r dr d\psi \\ &\text{subject to} \quad \Phi(r,\psi) = \exp\left(-\frac{r^2}{2\sigma(\psi)}\right), \\ &\qquad \frac{1}{4\pi^2}\int_0^{2\pi} \sigma(\psi) d\psi \le \alpha, \end{aligned} \tag{30}$$

where $\alpha \ge 0$ is a constant. Fig. 18(a) shows the TFD of the same 50% missing sample case after the AOK is applied. The artifacts due to missing samples are significantly reduced compared to the WVD depicted in Fig. 17(b).

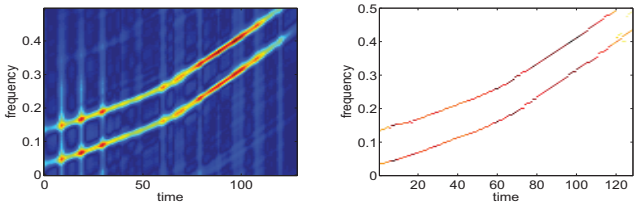

(a) TFD with AOK (b) OMP results

Fig. 18. TFD with 50% of missing samples obtained from AOK and the corresponding sparse reconstruction results using OMP.

3) Time-Frequency Representations through Sparse Reconstruction: Jammer TF sparse signature reconstruction builds upon the linear Fourier relationship between the TF domain and compressed observation domain. Depending on the specific domain representing the observation, the linear Fourier relationship may be 1-D or 2-D [53], [55]. In particular, the IAF and the TF representations are related by a 1-D DFT relationship. With this underlying linear model, a number of methods become available for the reconstruction of sparse FM jammer signals after proper TF kernels are applied. Orthogonal matching pursuit (OMP) is a method that allows specification of the number of jammer components in each time instant [58]. Recently, enhanced reconstruction of the FM signals with missing data is achieved by exploiting the contiguous structure of the FM signatures [54]. The proposed technique for jammer suppression under incomplete data builds on recent advances in TF analyses within the compressive sensing paradigm.

Denoting the kernelled AF in polar coordinates as $\tilde{A}(r,\psi) = A(r,\psi)\Phi(r,\psi)$, which is converted to the Cartesian coordinate system as $\tilde{A}(\zeta,\tau)$. Let $\mathbf{A}$ represent the AF matrix of $\tilde{A}(\zeta,\tau)$ with all ζ and τ entries. A conventional kernelled TFD matrix is obtained by a 2-D DFT of the kernelled AF matrix, expressed as

$$\mathbf{D} = \mathbf{F}_{\zeta}^{-\mathbf{1}}\mathbf{A}\mathbf{F}_{\tau}, \tag{31}$$

where $\mathbf{F}_z$ and $\mathbf{F}_z^{-1}$ respectively denote the DFT and IDFT matrices with resect to z. Alternatively, we can obtain the TFD through sparse reconstruction from $\mathbf{A}$. In this case, rather than utilizing the 2-D DFT relationship between the AF and the TFD as in [55], it is shown in [53], [54] that the 1-D DFT relationship between the IAF and the TFD yields simpler computations and, more importantly, enables the exploitation of local sparsity in the TF domain with respect to each time instant t.

The 1-D IDFT of $\mathbf{A}$ with respect to ζ results in the kernelled IAF matrix $\mathbf{C}$, which is represented with respect to time t and time delay τ,

$$\mathbf{C} = \mathbf{F}_{\zeta}^{-\mathbf{1}}\mathbf{A}. \tag{32}$$

Denote $\mathbf{c}^{[t]}$ as a column of matrix $\mathbf{C}$ corresponding to time t, and $\mathbf{u}^{[t]}$ as a vector contains all the TFD entries with respect to the frequency for the same time t. Then, the 1-D DFT relationship between the IAF and the TFD becomes

$$\mathbf{c}^{[t]} = \mathbf{F}_{\tau}\mathbf{u}^{[t]}, \tag{33}$$

for $0 \le t \le T-1$. This is a standard compressive sensing formulation and can be solved by a number of methods, such as the OMP, LASSO, and Bayesian compressive sensing. Fig. 18(b) shows the sparse TF representation, corresponding to Fig. 18(a), using the OMP method.

C. Jammer Suppression

We use the orthogonal projection scheme for effective jammer suppression. That is, the received signal vector, $\tilde{\mathbf{x}} = [x(0),\cdots,x(T-1)]^T$, is projected into the orthogonal subspace of the estimated jammers. Consider the estimated temporal signature of the lth jammer as

$$\hat{\mathbf{v}}_l = [\hat{v}_l(0),\cdots,\hat{v}_l(T-1)]^T. \tag{34}$$

Let $\mathbf{V}_J = [\hat{\mathbf{v}}_1,\cdots,\hat{\mathbf{v}}_L]$. The projection matrix into the orthogonal subspace of the jammers is given by [26]

$$\mathbf{P} = \mathbf{I}_{NT} - \mathbf{V}_J\left(\mathbf{V}_J^H\mathbf{V}_J\right)^{-1}\mathbf{V}_J^H. \tag{35}$$

The jammer-suppressed time-domain samples are expressed as the $T\times 1$ vector $\hat{\mathbf{x}} = \mathbf{P}\tilde{\mathbf{x}}$.

D. Suppression of Sparsely Sampled Jammer Signals

For the jammed GPS signal depicted in Figs. 17, the output SINR averaged over 20 independent trails, evaluated in each GPS symbol, is -0.72 dB. When the proposed technique is applied, the 128-sample data is divided into four segments in performing jammer suppression. Fig. 19(a) shows the resulting jammer waveform, and Fig. 19(b) shows the GPS signals before and after jammer suppression. It is evident that the jammers are substantially mitigated. The yielding output SINR averaged over the same 20 independent trails is 12.59 dB.

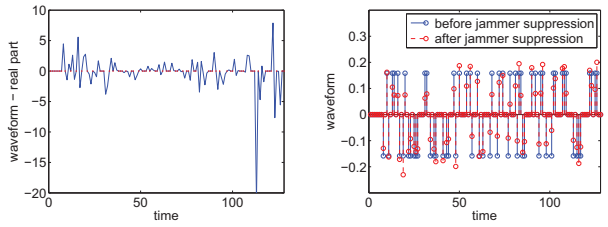

(a) Overall waveform (b) GPS signal waveforms

Fig. 19. Real-part waveform of the jammed signal after jammer suppression, and the GPS signals before and after jammer suppression.

VII. Conclusion

In this paper, we discussed the applications of sparse array design and sparse signal processing for the estimation of jammer signal structure and DOA. We reviewed recent developments in antenna selection techniques for the maximization of the beamforming SINR, for DOA estimation using CRB as the optimization metric. The coarray concept associated with autocorrelation computations for beamforming and DOA estimation was presented and applied to single and multiple CRPA receivers, showing enhanced jammer mitigation. When sparsity is exhibited in jammer signal representation, such as FM jammers in the TF domain, we demonstrated that effective jammer signal reconstruction is achievable under compressed observations that might result from random or missing sampling. Many open problems still remain in sparsity-aware anti-jam GNSS which should include full evaluation of multi-sensor receiver performance in terms of satellite signal acquisition and tracking in presence of smart jamming.

References

[1] A. Gecan and M. Zoltowski, "Power minimization techniques for GPS null steering antenna," in *Proceedings of the 8th International Technical Meeting of the Satellite Division of The Institute of Navigation (ION GPS 1995)*, pp. 861–868, 1995.

[2] M. Amin, L. Zhao, and A. Lindsey, "Subspace array processing for the suppression of FM jamming in GPS receivers," *Aerospace and Electronic Systems, IEEE Transactions on*, vol. 40, no. 1, pp. 80–92, 2004.

[3] W. Sun and M. Amin, "A self-coherence anti-jamming GPS receiver," *Signal Processing, IEEE Transactions on*, vol. 53, no. 10, pp. 3910–3915, 2005.

[4] M. Amin and W. Sun, "A novel interference suppression scheme for global navigation satellite systems using antenna array," *Selected Areas in Communications, IEEE Journal on*, vol. 23, no. 5, pp. 999–1012, 2005.

[5] M. Sahmoudi and M. Amin, "Optimal robust beamforming for interference and multipath mitigation in gnss arrays," in *Acoustics, Speech and Signal Processing, 2007. ICASSP 2007. IEEE International Conference on*, vol. 3, pp. III–693–III–696, April 2007.

[6] S. Daneshmand, A. Broumandan, and G. Lachapelle, "GNSS interference and multipath suppression using array antenna," in *Proceedings of the 24th International Technical Meeting of The Satellite Division of the Institute of Navigation (ION GNSS 2011)*, p. 1183, 2001.

[7] R. Fante and J. Vaccaro, "Wideband cancellation of interference in a GPS receive array," *Aerospace and Electronic Systems, IEEE Transactions on*, vol. 36, no. 2, pp. 549–564, 2000.

[8] S.-J. Kim and R. Iltis, "STAP for GPS receiver synchronization," *Aerospace and Electronic Systems, IEEE Transactions on*, vol. 40, pp. 132–144, Jan 2004.

[9] W. L. Myrick, J. Goldstein, and M. Zoltowski, "Low complexity anti-jam space-time processing for GPS," in *Acoustics, Speech, and Signal Processing, 2001. Proceedings. (ICASSP '01). 2001 IEEE International Conference on*, vol. 4, pp. 2233–2236 vol.4, 2001.

[10] R. L. Fante, M. P. Fitzgibbons, and K. F. McDonald, "Effect of adaptive array processing on GPS signal crosscorrelation," in *Proc. ION GNSS 2004*, pp. 579–583, 2004.

[11] J. Wang and M. Amin, "Multiple interference cancellation performance for GPS receivers with dual-polarized antenna arrays," *EURASIP Journal on Advances in Signal Processing*, vol. 2008, no. 1, p. 597613, 2008.

[12] W. Mu, M. Amin, and Y. Zhang, "Bilinear signal synthesis in array processing," *Signal Processing, IEEE Transactions on*, vol. 51, pp. 90–100, Jan 2003.

[13] A. Belouchrani and M. Amin, "Blind source separation based on time-frequency signal representations," *Signal Processing, IEEE Transactions on*, vol. 46, pp. 2888–2897, Nov 1998.

[14] A. Brown and D. Morley, "Test results of a 7-element small controlled reception pattern antenna," in *Proceedings of ION GPS*, pp. 1–8, 2001.

[15] X. Wang, E. Aboutanios, M. Trinkle, and M. Amin, "Reconfigurable adaptive array beamforming by antenna selection," *Signal Processing, IEEE Transactions on*, vol. 62, pp. 2385–2396, May 2014.

[16] R. Hoctor and S. Kassam, "The unifying role of the coarray in aperture synthesis for coherent and incoherent imaging," *Proceedings of the IEEE*, vol. 78, pp. 735–752, Apr 1990.

[17] S. Pillai and F. Haber, "Statistical analysis of a high resolution spatial spectrum estimator utilizing an augmented covariance matrix," *Acoustics, Speech and Signal Processing, IEEE Transactions on*, vol. 35, pp. 1517–1523, Nov 1987.

[18] P. Pal and P. Vaidyanathan, "Nested arrays: A novel approach to array processing with enhanced degrees of freedom," *Signal Processing, IEEE Transactions on*, vol. 58, pp. 4167–4181, Aug 2010.

[19] M. G. Amin, B. Jokanovic, Y. D. Zhang, and F. Ahmad, "A sparsity-perspective to quadratic time-frequency distributions," *Digital Signal Process.*, 2016 (in press).

[20] M. G. Amin and Y. D. Zhang, "Nonstationary jammer excision for GPS receivers using sparse reconstruction techniques," in *Proceedings of ION GNSS+*, (Tampa, FL, USA), pp. 3469–3474, Sept. 2014.

[21] A. Balaei and E. Aboutanios, "Characterization of interference effects in multiple antenna GNSS receivers," in *Image and Signal Processing (CISP), 2010 3rd International Congress on*, vol. 8, pp. 3930–3934, IEEE, 2010.

[22] M. Li, A. Dempster, A. Balaei, C. Rizos, and F. Wang, "Switchable beam steering/null steering algorithm for CW interference mitigation in GPS C/A code receivers," *Aerospace and Electronic Systems, IEEE Transactions on*, vol. 47, no. 3, pp. 1564–1579, 2011.

[23] X. Wang and E. Aboutanios, "Theoretical analysis of reconfigurable adaptive antenna array in GNSS applications," in *21st European Signal Processing Conference, Eusipco2013*, 9-13 Sep. 2013.

[24] X. Wang, E. Aboutanios, and M. G. Amin, "Generalised array reconfiguration for adaptive beamforming by antenna selection," in *Acoustics, Speech and Signal Processing (ICASSP), 2015 IEEE International Conference on*, pp. 2479–2483, IEEE, 2015.

[25] X. Wang, E. Aboutanios, and M. G. Amin, "Slow radar target detection in heterogeneous clutter using thinned space-time adaptive processing," *IET Radar, Sonar & Navigation*, November 2015.

[26] Y. Zhang and M. Amin, "Array processing for nonstationary interference suppression in DS/SS communications using subspace projection techniques," *Signal Processing, IEEE Transactions on*, vol. 49, pp. 3005–3014, Dec 2001.

[27] Y. Zhang, M. Amin, and B. Wang, "Mitigation of sparsely sampled nonstationary jammers for multi-antenna gnss receivers," in *Proceedings of 2016 IEEE International Conference on Acoustics, Speech and Signal Processing (ICASSP 2016)*, March 2016.

[28] D. S. Jimmy LaMance, "Locata correlator-based beam forming antenna technology for precise indoor positioning and attitude," in *Proceedings of the 24th International Technical Meeting of The Satellite Division of the Institute of Navigation (ION GNSS 2011), September 2011*, pp. 2436–2445, 2011.

[29] X. Wang, E. Aboutanios, and A. Dempster, "Low cost adaptive signal processing by subarray selection," in *2013 IGNSS Symposium*, 2013.

[30] X. Wang, M. Amin, F. Ahmad, and E. Aboutanios, "Bayesian compressive sensing for DOA estimation using the difference coarray," in *Acoustics, Speech and Signal Processing (ICASSP), 2015 IEEE International Conference on*, pp. 2384–2388, April 2015.

[31] J. Betz, "Effect of narrowband interference on GPS code tracking accuracy," in *Proceedings of the 2000 National Technical Meeting of The Institute of Navigation*, pp. 16–27, 2000.

[32] S. Boyd and L. Vandenberghe, *Convex Optimization*. Cambridge University Press, 2004.

[33] Y. Selén, H. Tullberg, and J. Kronander, "Sensor selection for cooperative spectrum sensing," in *New Frontiers in Dynamic Spectrum Access Networks, 2008. DySPAN 2008. 3rd IEEE Symposium on*, pp. 1–11, IEEE, 2008.

[34] A. Khabbazibasmenj and S. Vorobyov, "Robust adaptive beamforming for general-rank signal model with positive semi-definite constraint via potdc," *Signal Processing, IEEE Transactions on*, vol. 61, no. 23, pp. 6103–6117, 2013.

[35] X. Wang, E. Aboutanios, and M. Amin, "Adaptive array thinning for enhanced DOA estimation," *Signal Processing Letters, IEEE*, vol. 22, pp. 799–803, July 2015.

[36] W. Dinkelbach, "On nonlinear fractional programming," *Management Science*, vol. 13, no. 7, pp. 492–498, 1967.

[37] A. Moffet, "Minimum-redundancy linear arrays," *Antennas and Propagation, IEEE Transactions on*, vol. 16, no. 2, pp. 172–175, 1968.

[38] S. Pillai, Y. Bar-Ness, and F. Haber, "A new approach to array geometry for improved spatial spectrum estimation," *Proceedings of the IEEE*, vol. 73, pp. 1522–1524, Oct 1985.

[39] Y. Abramovich, N. Spencer, and A. Gorokhov, "Positive-definite toeplitz completion in doa estimation for nonuniform linear antenna arrays. ii. partially augmentable arrays," *Signal Processing, IEEE Transactions on*, vol. 47, pp. 1502–1521, Jun 1999.

[40] B. Friedlander and A. Weiss, "Direction finding using spatial smoothing with interpolated arrays," *Aerospace and Electronic Systems, IEEE Transactions on*, vol. 28, pp. 574–587, Apr 1992.

[41] Y. D. Zhang, M. G. Amin, and B. Himed, "Sparsity-based DOA estimation using co-prime arrays," in *Acoustics, Speech, and Signal Processing, 2013. Proceedings. (ICASSP '13). 2013 IEEE International Conference on*, (Vancouver, Canada), pp. 1–5, May 2013.

[42] J. F. de Andrade, Jr., M. L. R. de Campos, and J. A. Apolinario, Jr., "A complex version of the lasso algorithm and its application to beamforming," in *The 7th International Telecommunications Symposium (ITS 2010)*, 2010.

[43] D. Malioutov, M. Cetin, and A. Willsky, "A sparse signal reconstruction perspective for source localization with sensor arrays," *Signal Processing, IEEE Transactions on*, vol. 53, no. 8, pp. 3010–3022, 2005.

[44] S.-J. Kim, K. Koh, M. Lustig, S. Boyd, and D. Gorinevsky, "An interior-point method for large-scale l1-regularized least squares," *Selected Topics in Signal Processing, IEEE Journal of*, vol. 1, pp. 606–617, Dec 2007.

[45] M. Amin, "Concurrent nulling and locations of multiple interferences in adaptive antenna arrays," *Signal Processing, IEEE Transactions on*, vol. 40, pp. 2658–2668, Nov 1992.

[46] Y. Zhang and M. Amin, "Anti-jamming GPS receiver with reduced phase distortions," *Signal Processing Letters, IEEE*, vol. 19, pp. 635–638, Oct 2012.

[47] B. Friedlander and B. Porat, "Performance analysis of a null-steering algorithm based on direction-of-arrival estimation," *Acoustics, Speech and Signal Processing, IEEE Transactions on*, vol. 37, pp. 461–466, April 1989.

[48] A. Haimovich and Y. Bar-Ness, "An eigenanalysis interference canceler," *Signal Processing, IEEE Transactions on*, vol. 39, no. 1, pp. 76–84, 1991.

[49] M. G. Amin, "Interference mitigation in spread spectrum communication systems using time-frequency distributions," *IEEE Trans. Signal Process.*, vol. 45, no. 1, pp. 90–101, 1997.

[50] B. Boashash, "Estimating and interpreting the instantaneous frequency of a signal," *Proc. IEEE*, vol. 80, pp. 520–538, 1990.

[51] H. Zhang, G. Bi, W. Yang, S. G. Razul, and C.-M. S. See, "IF estimation of FM signals based on time-frequency image," *IEEE Trans. Aerospace Electron. Syst.*, vol. 51, pp. 326–343, 2015.

[52] L. Liu and M. G. Amin, "Performance analysis of GPS receivers in non-Gaussian noise incorporating pre-correlation filter and sampling rate," *IEEE Trans. Signal Proc.*, vol. 56, pp. 990–1004, 2008.

[53] Y. Zhang, M. G. Amin, and B. Himed, "Reduced interference time-frequency representations and sparse reconstruction of undersampled data," in *Proceedings of EUSIPCO*, (Marrakech, Morocco), pp. 1–5, Sept. 2013.

[54] Q. Wu, Y. Zhang, and M. G. Amin, "Continuous structure based Bayesian compressive sensing for sparse reconstruction of time-frequency distribution," in *Proceedings of Int. Conf. Digital Signal Proc.*, (Hong Kong, China), pp. 831–836, Aug. 2014.

[55] P. Flandrin and P. Borgnat, "Time-frequency energy distributions meet compressed sensing," *IEEE Trans. Signal Process.*, vol. 58, pp. 2974–2982, 2010.

[56] L. Cohen, *Time Frequency Analysis: Theory and Applications*. Prentice-Hall, first ed., 1994.

[57] R. G. Baraniuk and D. L. Jones, "A signal-dependent time-frequency representation: Optimal kernel design," *IEEE Trans. Signal Process.*, vol. 41, pp. 1589–1602, 1993.

[58] J. Tropp and A. Gilbert, "Signal recovery from random measurements via orthogonal matching pursuit," *Information Theory, IEEE Transactions on*, vol. 53, pp. 4655–4666, Dec 2007.

Moeness G. Amin (F'01) is the Director of the Center for Advanced Communications, Villanova University, Pennsylvania, USA. He is a Fellow of the Institute of Electrical and Electronics Engineers; Fellow of the International Society of Optical Engineering; Fellow of the Institute of Engineering and Technology; and Fellow of the European Association for Signal Processing. Dr. Amin is a Recipient of the 2014 IEEE Signal Processing Society Technical Achievement Award; Recipient of the 2009 Individual Technical Achievement Award from the European Association for Signal Processing; Recipient of the IEEE Warren D White Award for Excellence in Radar Engineering; Recipient of the IEEE Third Millennium Medal; Recipient of the 2010 NATO Scientific Achievement Award; Recipient of the 2010 Chief of Naval Research Challenge Award; Recipient of Villanova University Outstanding Faculty Research Award, 1997; and the Recipient of the IEEE Philadelphia Section Award, 1997. He was a Distinguished Lecturer of the IEEE Signal Processing Society, 2003-2004, and is currently the Chair of the Electrical Cluster of the Franklin Institute Committee on Science and the Arts. Dr. Amin has over 700 journal and conference publications in signal processing theory and applications. He co-authored 20 book chapters and is the Editor of the three books "Through the Wall Radar Imaging", "Compressive Sensing for Urban Radar," and "Radar for Indoor Monitoring" published by CRC Press in 2011, 2014, 2017, respectively.

Xiangrong Wang Xiangrong Wang received the Ph.D. degree in electrical engineering from University of New South Wales (UNSW), Australia, in June 2015. She was awarded a Postdoctoral Writing Fellowship by UNSW to the end of 2015. She is currently a postdoctoral research fellow in the Center for Advanced Communications, Villanova University. Her research interests include adaptive array processing, DOA estimation and convex optimization.

Yimin D. Zhang (SM'01) received his Ph.D. degree from the University of Tsukuba, Tsukuba, Japan, in 1988. He joined the faculty of the Department of Radio Engineering, Southeast University, Nanjing, China, in 1988. He served as a Director and Technical Manager at the Oriental Science Laboratory, Yokohama, Japan, from 1989 to 1995, a Senior Technical Manager at the Communication Laboratory Japan, Kawasaki, Japan, from 1995 to 1997, and a Visiting Researcher at the ATR Adaptive Communications Research Laboratories, Kyoto, Japan, from 1997 to 1998. He was with the Villanova University, Villanova, PA, from 1998 to 2015, where he was a Research Professor with the Center for Advanced Communications. Since 2015, he has been with the Department of Electrical and Computer Engineering, College of Engineering, Temple University, Philadelphia, PA, where he is currently an Associate Professor. His general research interests lie in the areas of statistical signal and array processing applied for radar, communications, and navigation, including compressive sensing, convex optimization, time-frequency analysis, MIMO system, radar imaging, target localization and tracking, wireless networks, and jammer suppression. He has published 280 journal articles and conference papers and 12 book chapters. Dr. Zhang is an Associate Editor for the IEEE Transactions on Signal Processing, and serves on the Editorial Board of the Signal Processing journal. He was an Associate Editor for the IEEE Signal Processing Letters during 20062010, and an Associate Editor for the Journal of the Franklin Institute during 20072013. He is a member of the Sensor Array and Multichannel Technical Committee of the IEEE Signal Processing Society.

Fauzia Ahmad (SM'06) received her Ph.D. degree in electrical engineering from the University of Pennsylvania, Philadelphia, PA in 1997. Since 2002, she has been with the Villanova University, Villanova, PA, where she is currently a Research Professor with the Center for Advanced Communications in the College of Engineering,and is the Director of the Radar Imaging Laboratory. She is a Senior Member of the IEEE and the SPIE. Her general research interests are in the areas of statistical signal and array processing, radar imaging, radar signal processing, compressive sensing, waveform diversity and design, target localization and tracking, direction finding, and ultrasound imaging. She has published more than 190 journal articles and peer-reviewed conference papers and six book chapters in the aforementioned areas. Dr. Ahmad is an Associate Editor of the IEEE Transactions on Signal processing and IEEE Geoscience and Remote Sensing Letters, and serves on the editorial board of IET Radar, Sonar, and Navigation and SPIE/IS&T Journal of Electronic Imaging. She is a member of the IEEE Aerospace and Electronic System Society's Radar Systems Panel, IEEE Signal Processing Society's Sensor Array and Multichannel Technical Committee, and the Electrical Cluster of the Franklin Institute Committee on Science and the Arts. She also chairs the SPIE Conference Series on Compressive Sensing. Dr.Ahmad is the Lead Guest Editor of IEEE Signal Processign Magazine March-2016 Special Issue on Signal Processing for Assisted Living. She was the Lead Guest Editor of the SPIE/IS&T Journal of Electronic Imaging April-June 2013 Special Section on Compressive Sensing for Imaging and the Lead Guest Editor of the IET Radar, Sonar& Navigation February-2015 Special Issue on Radar Applied to Remote Patient Monitoring and Eldercare.

Elias Aboutanios received a Bachelor in Engineering in 1997, from the University of New South Wales (UNSW) and the PhD degree in 2003, from the University of Technology, Sydney (UTS), Australia. From 2003 until 2007, he was a research fellow at the University of Edinburgh. Since 2007, he has been a faculty member at the School of Electrical Engineering and Telecommunications at UNSW. Dr Aboutanios was awarded the UNSW Co-op Scholarship in 1993, and the following year he was the recipient of the Sydney Electricity scholarship. In 1998, he was awarded the Australian Postgraduate Scholarship and commenced his work toward the PhD degree at UTS. While at UTS he was a member of the Cooperative Research Center for Satellite Systems team, working on the Ka Band Earth station. In 2011, he received the Faculty of Engineerings Teaching Excellence Award, and in 2014, he was awarded an Excellence in Research Supervision award. In 2011, he led a consortium comprising Thales Alenia Space, Optus, ISAE and UNSW to secure over $1M in funding to develop Australias first masters program in Satellite Systems Engineering. He also established and leads the UNSW-EC0 project at UNSW to build a 2Unit cubesat for the European QB50 project. Dr Aboutanios is the UNSW IEEE student branch counselor and mentor for the BLUEsat student team. He is an Associate Editor on the IET Signal Processing Journal and lead guest editor for the Eurasip Journal on Advances in Signal Processing special issue on "Biologically Inspired Signal Processing: Analyses, Algorithms and Applications". He has been awarded the best oral presentation award at the 3rd International Congress on Image and Signal Processing in 2010. His research interests include parameter estimation, algorithm optimization and analysis, adaptive and statistical signal processing and their application in the contexts of radar, Nuclear Magnetic Resonance, and communications. He has over 70 journal and conference publications and is the joint holder of a patent on frequency estimation.